MOLECULAR ELECTRONICS

High-performance transistors for bioelectronics through tuning of channel thickness

10.1126/sciadv.1400251

Jonathan Rivnay,[1] Pierre Leleux,[1,2] Marc Ferro,[1] Michele Sessolo,[1]* Adam Williamson,[3,4] Dimitrios A. Koutsouras,[1] Dion Khodagholy,[1†] Marc Ramuz,[1] Xenofon Strakosas,[1] Roisin M. Owens,[1] Christian Benar,[3,4] Jean-Michel Badier,[3,4] Christophe Bernard,[3,4] George G. Malliaras[1‡]

Despite recent interest in organic electrochemical transistors (OECTs), sparked by their straightforward fabrication and high performance, the fundamental mechanism behind their operation remains largely unexplored. OECTs use an electrolyte in direct contact with a polymer channel as part of their device structure. Hence, they offer facile integration with biological milieux and are currently used as amplifying transducers for bioelectronics. Ion exchange between electrolyte and channel is believed to take place in OECTs, although the extent of this process and its impact on device characteristics are still unknown. We show that the uptake of ions from an electrolyte into a film of poly(3,4-ethylenedioxythiophene) doped with polystyrene sulfonate (PEDOT:PSS) leads to a purely volumetric capacitance of 39 F/cm^3. This results in a dependence of the transconductance on channel thickness, a new degree of freedom that we exploit to demonstrate high-quality recordings of human brain rhythms. Our results bring to the forefront a transistor class in which performance can be tuned independently of device footprint and provide guidelines for the design of materials that will lead to state-of-the-art transistor performance.

INTRODUCTION

Organic electrochemical transistors (OECTs) are the focus of intense development for applications in bioelectronics (*1*, *2*). Most of these devices use a conducting polymer film as their channel and are gated through an aqueous electrolyte, thereby offering intimate interfacing between solid-state electronics and biological milieux (*3*). Advantages such as straightforward fabrication, compatibility with low-cost printing techniques (including screen and inkjet printing) (*4*, *5*), compatibility with a wide range of substrates [including fibers (*6*) and paper (*7*)], and stability in aqueous environments have motivated their use in a variety of biosensing applications (*8*). OECTs have been used to detect ions (*9*, *10*), metabolites (*11*, *12*), hormones (*13*), DNA (*14*), and pathogenic organisms (*15*); probe cell adhesion (*16*); measure the integrity of barrier tissue (*17*); and interface with electrically active cells and tissues (*18*–*20*). Recent work highlighted the fact that OECTs show the largest transconductance among electrolyte-gated transistors (*21*). The transconductance is defined as $g_m = \partial I_D/\partial V_G$, where I_D is the drain current and V_G is the gate voltage, and, for bio-interfacing, quantifies the "efficiency" of transduction of a biological event (*22*). At the same time, it was shown that through microfabrication, OECTs can achieve a response time, τ, well below a millisecond, sufficient for most biosensing applications (*23*). Therefore, OECTs make powerful amplifying transducers, a fact demonstrated in applications including recordings of brain activity in rats (*24*) and electrochemical detection of neurotransmitters (*25*).

The operation of the OECT is distinctly different than that of the more traditional field-effect transistor (FET). The electrostatic coupling of the gate to the channel in a FET is described by the capacitance per unit area, C_i, of the gate dielectric. C_i is inversely proportional to the thickness of the gate dielectric and hence can be maximized by using an electrolyte to gate the channel, in which case the double layer created by ion accumulation at the surface of the channel leads to values around 5 μF/cm^2 (*26*). However, in OECTs, ionic charge is presumed to penetrate within the channel, a notion supported by the strong color change associated with switching an OECT between the ON and OFF states (*27*). Therefore, capacitance per unit area is an insufficient parameter for describing OECT operation. The lack of a proper description hinders our ability to optimize OECTs for biological applications, which is especially true given the broad range of requirements imposed by the different signals of interest.

RESULTS

We measured the electrochemical impedance of channels with width, *W*, and length, *L*, varying from 5 to 250 μm and channel thickness, *d*, from 20 nm to >1 μm (fig. S1A) and fit the spectra with an equivalent circuit consisting of a capacitor, *C*, describing the effective capacitance of the channel in parallel with a resistor, R_p, and in series with a resistor, R_s. This was the simplest circuit that could fit the entire data set. As shown in Fig. 1A and fig. S2, capacitance scales with the volume of the PEDOT:PSS [poly(3,4-ethylenedioxythiophene) doped with polystyrene sulfonate] film over a range of almost four orders of magnitude. This result implies that the ionic charge injected from the electrolyte is uniformly distributed within the PEDOT:PSS film (in the absence of a source-drain voltage), down to 10 μm^3. This agrees with our understanding of the structure of PEDOT:PSS, which is believed to consist of PEDOT:PSS-rich regions of the order of tens of nanometers surrounded by a PSS-rich phase (*28*–*30*). The line in Fig. 1A is a fit to a linear function with a zero offset, yielding a capacitance per unit

[1]Department of Bioelectronics, École Nationale Supérieure des Mines, CMP-EMSE, MOC, 13541 Gardanne, France. [2]MicroVitae Technologies, Pôle d'Activité Y. Morandat, 1480 rue d'Arménie, 13120 Gardanne, France. [3]Aix-Marseille Université, Institut de Neurosciences des Systèmes, 13005 Marseille, France. [4]INSERM, UMR_S 1106, 13005 Marseille, France.
*Present address: Instituto de Ciencia Molecular, Universitat de València, C/Catedrático José Beltrán 2, 46980 Paterna, Spain.
†Present address: NYU Neuroscience Institute, School of Medicine, New York University, New York, NY 10016, USA.
‡Corresponding author. E-mail: malliaras@emse.fr

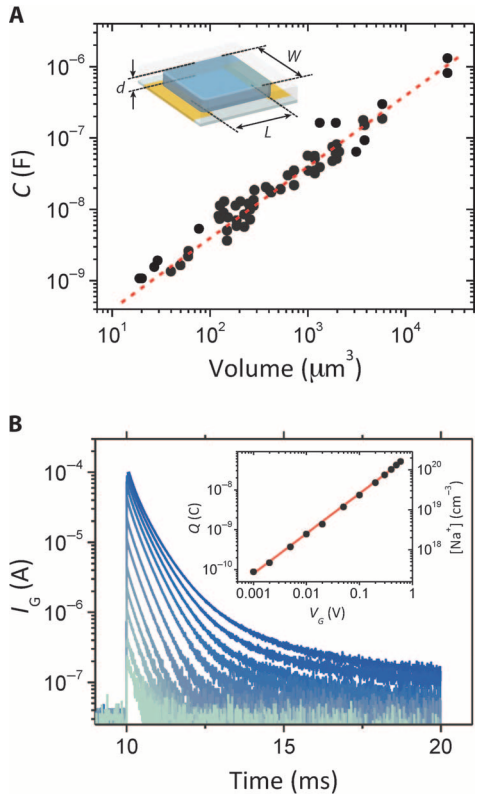

Fig. 1. Volumetric response in OECTs. (**A**) PEDOT:PSS capacitance determined from impedance spectroscopy (fig. S1) for devices of varying geometry. Inset: OECT configuration and channel dimensions (*W*, *L*, and *d*). The linear fit ($r^2 = 0.94$) to the capacitance data (red dotted line) yields a $C^* = 39.3 \pm 1.3$ F/cm^3. (**B**) Gate current transients from an OECT with nominal dimensions $W = 50$ μm, $L = 50$ μm, and $d = 500$ nm, for different values of applied gate voltage. The measured volume, including overlap with contacts, is 1.97×10^{-9} cm^3. Inset: Injected charge (*Q*) and sodium ion density as a function of V_G. The line is a fit ($r^2 = 0.99$), yielding a capacitance of 82.2 ± 0.8 nF.

volume, $C^* = 39.3 \pm 1.3$ F/cm^3. This value can be put in perspective by calculating that a 130-nm-thick PEDOT:PSS film has an equivalent capacitance per unit area of 500 μF/cm^2, which is 100 times larger than the double-layer capacitance. The dependence of capacitance on volume constitutes direct evidence for ion penetration in the channel of OECTs, whereas the zero offset signifies the absence of any ion accumulation at the surface, indicating a negligible ion injection barrier from the electrolyte into the conducting polymer film. This suggests that C^* as opposed to C_i is the appropriate parameter to describe the physics of these devices. Indeed, the value of C^* can be used to predict the ionic charge that is injected in the channel of an OECT. Figure 1B shows gate current transients from an OECT for different values of gate bias. The ionic charge injected in the channel was calculated from the area under these curves and is shown in the inset of Fig. 1B. The line is a fit corresponding to a capacitance per unit volume of 41.7 F/cm^3, a value that is within 7% of the one measured with impedance spectroscopy.

The volumetric response of capacitance leads to a particular dependence of the transconductance on device geometry. We measured the transconductance both at its peak for a fixed drain voltage and at saturation for a fixed gate voltage (see fig. S3B). The best correlation was found when the data were plotted against $W{\cdot}d/L$, as shown in Fig. 2A. This was found to hold both for the peak transconductance (open circles) and for the transconductance at saturation (solid circles). The line in Fig. 2A is a fit to a linear function, indicating that the transconductance at saturation is proportional to $W{\cdot}d/L$. This trend can be understood by introducing the notion of volumetric capacitance in a model describing transistor operation. Indeed, as shown in the Supplementary Materials, the transconductance in the saturation regime is given by:

$$g_m = (W \cdot d/L) \cdot \mu \cdot C^* \cdot (V_T - V_G) \quad (1)$$

where μ is the hole mobility in the PEDOT:PSS channel and V_T is a geometry-independent threshold voltage. This equation explicitly shows the scaling of transconductance with $W{\cdot}d/L$ and confirms the importance of C^* as a key parameter for describing OECT operation. It also highlights the difference between an OECT and an FET:

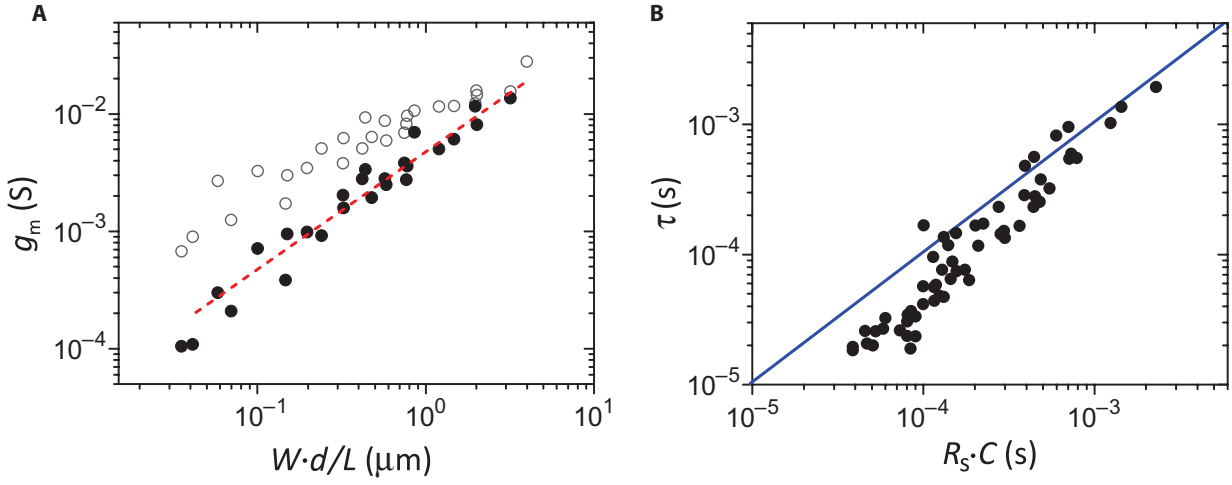

Fig. 2. Scaling of OECT metrics with channel geometry. (**A**) Scaling of OECT transconductance. Open symbols correspond to peak transconductance [at V_D (drain voltage) = −0.5 V and V_G that corresponds to maximum transconductance], and solid symbols are the transconductance at saturation (at $V_G = 0.4$ V and V_D that corresponds to saturation). The line is a linear fit ($r^2 = 0.96$) to the transconductance at saturation (Eq. 1). (**B**) Correlation between OECT response time, obtained from drain current transients, and $R_S{\cdot}C$ time, obtained by impedance spectroscopy. The line is a guide to the eye with a slope of 1 and represents the expected behavior $\tau = R_S{\cdot}C$.

the transconductance of the latter is described by substituting $d \cdot C^*$ with C_i in Eq. 1 and is not dependent on channel thickness.

The volumetric response of capacitance also affects the dependence of response time, τ, on device geometry. The response time of an OECT can be determined either by the redistribution of ionic charge in the gate circuit or by the time of flight of holes in the channel (*3*). We determined τ by fitting the drain current transient caused by a voltage pulse at the gate (see fig. S3C). According to the shape of the transient (*3*), it is the redistribution of the ionic charge that governs the response time of the OECTs. Indeed, as seen in Fig. 2B, τ follows the trend of $R_s \cdot C$, determined by impedance measurements. The difference observed for small devices is due to the fact that the $R_s \cdot C$ time was determined for the PEDOT:PSS film, which is a few micrometers longer than L to ensure overlap with the source and drain electrodes. Therefore, the response time is thickness-dependent, because C scales with film volume and R_s scales with film area (fig. S1B). This is different than in FETs, in which C_i is independent of channel thickness. It should be noted that the hole mobility, determined by driving the transistors with constant gate current (see fig. S4), was found to be 1.9 ± 1.3 cm^2/V · s, confirming that the time of flight of holes across the channel is faster than the OECT response time.

The dependence of transconductance on channel thickness can be used to tune transistor performance, as demonstrated here for the case of electroencephalography (EEG) recordings. EEG uses electrodes placed on the scalp to measure electric field oscillations that arise from the synchronous activity of neural networks in the brain (*31*) and is one of the most frequently used techniques for understanding human brain function and dysfunction, including epilepsy (*32*), Alzheimer's disease (*33*), and Parkinson's disease (*34*). We recorded EEG on a human volunteer with two OECTs connected as shown in Fig. 3A, using the brain as the supply of gate voltage. The two OECT channels had identical dimensions of W = 50 μm and L = 50 μm but a thickness of 230 and 870 nm, respectively. This resulted in a ~2× difference in apparent transconductance (not corrected for resistive loss on interconnects) and allowed for identical electronics, set to the same range, to record the drain current of both the thin and the thick devices, thereby removing from the comparison any extraneous factors related to differences in signal acquisition and treatment. Typical traces from the OECTs with the thick (blue) and thin (red) channels are shown in Fig. 3B. The corresponding spectral analysis shows a peak around 10 Hz, corresponding to typical α rhythms, which are indicative of wakeful relaxation (Fig. 3C) (*35*). The two spectra reveal an enhanced signal with richer content below the primary α band for the OECT with the thick channel. There is a 16-dB enhancement in power using the thicker channel, consistent with the hypothesis that the transistor with the higher transconductance (inset) provides better low-frequency recordings. Oscillatory activity at such low frequencies (1 to 8 Hz) is clinically important because it is a classical marker of lesional tissues (*36*).

DISCUSSION

The scaling of transconductance with channel thickness represents a major difference between electrochemical transistors and FETs and can be used henceforth as the identifying characteristic of OECTs. This scaling was found to hold for films with a thickness up to >1 μm. It is conceivable that deviations from this scaling may occur in thicker films due to second-order effects (for example, incomplete film hydration), but we did not explore this regime. As demonstrated for the case of EEG recordings, thickness can be used to tune transconductance, and hence performance, independently of device footprint. This makes OECTs ideal candidates for applications in which channel area is fixed by geometrical constraints, such as recording arrays, where devices must be closely packed, and lab-on-a-chip systems, where space is very tight. In addition to device geometry, Eq. 1 shows that transconductance is determined by the product of hole mobility and capacitance per unit volume ($\mu \cdot C^*$). Concerning the dependence of hole mobility on the

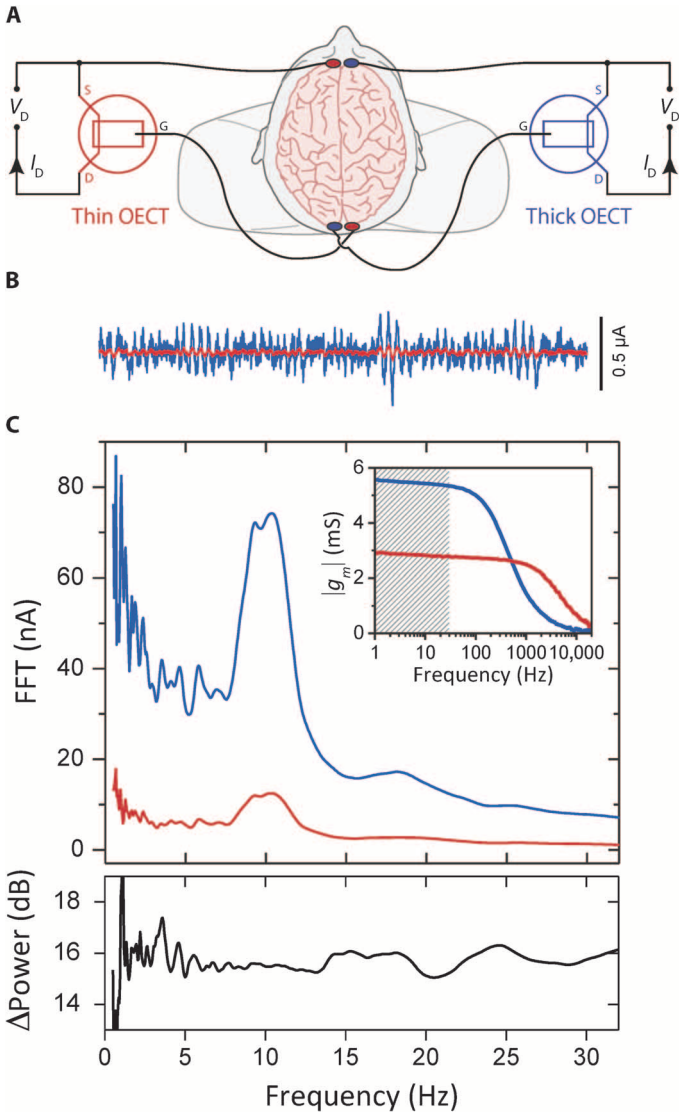

Fig. 3. Human EEG recordings enhanced with high-transconductance OECTs. (**A**) Wiring diagram of two OECTs simultaneously used as transducers to record human EEG signals, where V_D = −0.6 V. (**B**) Six-second recordings from a thick (blue) and thin (red) OECT showing α rhythms. (**C**) Top: Spectral analysis of simultaneous 60-s EEG recordings (transconductance frequency response is shown in the inset; shaded band corresponds to EEG-relevant frequencies). The power enhancement of the recording from the thick device compared to the thin device is plotted at the bottom, showing the enhanced low-frequency signal when using the thick device and the richer spectral content below the primary α band. FFT, fast Fourier transform.

structure of conjugated polymers, it is known that enhanced π-π interactions via crystallite or aggregate formation and better intergrain connectivity improve electronic charge transport (*37*). The value of 1.9 ± 1.3 $cm^2/V{\cdot}s$ obtained for PEDOT:PSS implies the existence of an efficient pathway for hole transport, consistent with recent measurements in electrochemically gated polythiophene (*38*). On the other hand, little is known about the dependence of C^* on the structure of conducting polymers. Although volumetric charge storage is important for a variety of applications, including electrolytic capacitors and batteries, interest has focused on gravimetric rather than volumetric capacitance. To the best of our knowledge, there are no previous measurements that explicitly show capacitance scaling with sample volume. A volumetric capacitance of 376 F/cm^3, an order of magnitude higher than that measured here for PEDOT:PSS, was recently reported in a porous carbon (*39*). From literature data for poly(3-hexylthiophene), we estimate values ranging from 3 (*40*) to 200 F/cm^3 (*38*), although one should note that these values come from single samples and might be overestimated because of stray capacitances and ion accumulation at the film/electrolyte interface. This wide range of values implies that film structure plays a major role in determining C^*. Moreover, recent measurements in PEDOT:PSS suggest that hydration is important for ion transport (*41*). This implies that the ability of a material to take up water and swell is important for a large C^*. Therefore, it seems that maximizing $\mu{\cdot}C^*$ requires a balancing act: dense aggregation and/or crystallinity for efficient hole transport versus a loose, hierarchical, and open packing for facile ion transport. The combination of two phases in PEDOT:PSS, an aggregating and interconnected phase (PEDOT:PSS-rich) that provides efficient hole transport and an amorphous phase (PSS) that can easily hydrate and transport ions, may be the reason why PEDOT:PSS is the champion material for OECTs. We expect that future work will explore the dependence of $\mu{\cdot}C^*$ on the chemical nature and structure of organic films, leading to better materials and devices for bioelectronics.

MATERIALS AND METHODS

OECTs were fabricated in a clean room and patterned using photolithography. They consisted of a PEDOT:PSS channel [Clevios PH 1000 from Heraeus Holding GmbH, with 5 volume % ethylene glycol, 0.1 volume % dodecyl benzene sulfonic acid, and 1 wt % of (3-glycidyloxypropyl)trimethoxysilane)] with Au source and drain electrodes and interconnect lines. A parylene C layer was used to insulate the Au interconnects from the electrolyte. Care was taken to ensure that the voltage drop along the interconnects was negligible or was accounted for in the analysis of electrical characteristics by correcting the applied voltage for resistive loss. PEDOT:PSS film area, channel width, and channel length of small devices were measured with optical microscopy; channel thickness was measured with a mechanical profilometer and/or an atomic force microscope; and these measured values were taken into account in data analysis. NaCl (100 mM) in deionized water was used as the electrolyte, and a Ag/AgCl pellet (Warner Instruments) as the gate electrode. Electrical measurements followed previously defined protocols, and the output curves were measured slowly enough to allow steady state to be reached. A three-electrode configuration was used for the impedance spectroscopy measurements (Metrohm), with platinum and Ag/AgCl counter and reference electrodes, respectively. The source and drain electrodes are shorted together, and the channel was used as the working electrode.

All human volunteers provided informed signed consent to participate in the study. Commercially available Ag/AgCl electrodes (Comepa Industries) connected the gate and source of the OECTs to the scalp of the volunteer. The OECTs used a Ag/AgCl gate electrode (Warner Instruments) and a 100 mM NaCl in DI water as the electrolyte. The drain current was measured using a National Instruments PXIe-1062Q system equipped with a PXIe-4145 source measure unit (SMU) that was used to bias the two OECTs and record the drain currents with a sampling rate of 1 kHz. The drain currents were simultaneously recorded using the same range on the two SMUs to ensure an accurate comparison. The EEG recordings were analyzed using custom MATLAB tools (MathWorks). The recordings were digitally filtered using a 0.1-Hz high-pass filter. Spectral analysis was performed using a Gabor wavelet time–frequency analysis, and frequency power was used for device performance comparison.

SUPPLEMENTARY MATERIALS

Supplementary materials for this article are available at http://advances.sciencemag.org/cgi/content/full/1/4/e1400251/DC1

Fig. S1. Impedance spectroscopy.
Fig. S2. Thickness dependence of capacitance.
Fig. S3. Device characteristics of typical OECT.
Fig. S4. Determination of hole mobility from drain current transients.
Table S1. Hole mobility values for OECTs of different geometry.

REFERENCES AND NOTES

1. M. Berggren, A. Richter-Dahlfors, Organic bioelectronics. *Adv. Mater.* **19**, 3201–3213 (2007).
2. J. Rivnay, R. M. Owens, G. G. Malliaras, The rise of organic bioelectronics. *Chem. Mater.* **26**, 679–685 (2014).
3. D. A. Bernards, G. G. Malliaras, Steady-state and transient behavior of organic electrochemical transistors. *Adv. Funct. Mater.* **17**, 3538–3544 (2007).
4. D. Nilsson, M. Chen, T. Kugler, T. Remonen, M. Armgarth, M. Berggren, Bi-stable and dynamic current modulation in electrochemical organic transistors. *Adv. Mater.* **14**, 51–54 (2002).
5. L. Basiricò, P. Cosseddu, A. Scidà, B. Fraboni, G. G. Malliaras, A. Bonfiglio, Electrical characteristics of ink-jet printed, all-polymer electrochemical transistors. *Org. Electron.* **13**, 244–248 (2012).
6. M. Hamedi, R. Forchheimer, O. Inganäs, Towards woven logic from organic electronic fibres. *Nat. Mater.* **6**, 357–362 (2007).
7. D. Nilsson, T. Kugler, P.-O. Svensson, M. Berggren, An all-organic sensor–transistor based on a novel electrochemical transducer concept printed electrochemical sensors on paper. *Sens. Actuators B* **86**, 193–197 (2002).
8. P. Lin, F. Yan, Organic thin-film transistors for chemical and biological sensing. *Adv. Mater.* **24**, 34–51 (2012).
9. P.-O. Svensson, D. Nilsson, R. Forchheimer, M. Berggren, A sensor circuit using reference-based conductance switching in organic electrochemical transistors. *Appl. Phys. Lett.* **93**, 203301 (2008).
10. M. Sessolo, J. Rivnay, E. Bandiello, G. G. Malliaras, H. J. Bolink, Ion-selective organic electrochemical transistors. *Adv. Mater.* **26**, 4803–4807 (2014).
11. Z. T. Zhu, J. T. Mabeck, C. Zhu, N. C. Cady, C. A. Batt, G. G. Malliaras, A simple poly(3,4-ethylene dioxythiophene)/poly(styrene sulfonic acid) transistor for glucose sensing at neutral pH. *Chem. Commun.*, 1556–1557 (2004).
12. H. Tang, F. Yan, P. Lin, J. Xu, H. L. W. Chan, Highly sensitive glucose biosensors based on organic electrochemical transistors using platinum gate electrodes modified with enzyme and nanomaterials. *Adv. Funct. Mater.* **21**, 2264–2272 (2011).
13. N. Coppedè, G. Tarabella, M. Villani, D. Calestani, S. Iannotta, A. Zappettini, Human stress monitoring through an organic cotton-fiber biosensor. *J. Mater. Chem. B* **2**, 5620–5626 (2014).
14. P. Lin, X. Luo, I. M. Hsing, F. Yan, Organic electrochemical transistors integrated in flexible microfluidic systems and used for label-free DNA sensing. *Adv. Mater.* **23**, 4035–4040 (2011).
15. R.-X. He, M. Zhang, F. Tan, P. H. M. Leung, X.-Z. Zhao, H. L. W. Chan, M. Yang, F. Yan, Detection of bacteria with organic electrochemical transistors. *J. Mater. Chem.* **22**, 22072–22076 (2012).
16. P. Lin, F. Yan, J. Yu, H. L. W. Chan, M. Yang, The application of organic electrochemical transistors in cell-based biosensors. *Adv. Mater.* **22**, 3655–3660 (2010).

17. L. H. Jimison, S. A. Tria, D. Khodagholy, M. Gurfinkel, E. Lanzarini, A. Hama, G. G. Malliaras, R. M. Owens, Measurement of barrier tissue integrity with an organic electrochemical transistor. *Adv. Mater.* **24**, 5919–5923 (2012).
18. A. Campana, T. Cramer, D. T. Simon, M. Berggren, F. Biscarini, Electrocardiographic recording with conformable organic electrochemical transistor fabricated on resorbable bioscaffold. *Adv. Mater.* **26**, 3874–3878 (2014).
19. P. Leleux, J. Rivnay, T. Lonjaret, J. M. Badier, C. Bénar, T. Hervé, P. Chauvel, G. G. Malliaras, Organic electrochemical transistors for clinical applications. *Adv. Healthc. Mater.* **4**, 142–147 (2015).
20. C. Yao, Q. Li, J. Guo, F. Yan, I. M. Hsing, Rigid and flexible organic electrochemical transistor arrays for monitoring action potentials from electrogenic cells. *Adv. Healthc. Mater.* **4**, 528–533 (2014).
21. D. Khodagholy, J. Rivnay, M. Sessolo, M. Gurfinkel, P. Leleux, L. H. Jimison, E. Stavrinidou, T. Herve, S. Sanaur, R. M. Owens, G. G. Malliaras, High transconductance organic electrochemical transistors. *Nat. Commun.* **4**, 2133 (2013).
22. J. Rivnay, P. Leleux, M. Sessolo, D. Khodagholy, T. Hervé, M. Fiocchi, G. G. Malliaras, Organic electrochemical transistors with maximum transconductance at zero gate bias. *Adv. Mater.* **25**, 7010–7014 (2013).
23. D. Khodagholy, M. Gurfinkel, E. Stavrinidou, P. Leleux, T. Herve, S. Sanaur, G. G. Malliaras, High speed and high density organic electrochemical transistor arrays. *Appl. Phys. Lett.* **99**, 163304 (2011).
24. D. Khodagholy, T. Doublet, P. Quilichini, M. Gurfinkel, P. Leleux, A. Ghestem, E. Ismailova, T. Hervé, S. Sanaur, C. Bernard, G. G. Malliaras, In vivo recordings of brain activity using organic transistors. *Nat. Commun.* **4**, 1575 (2013).
25. K. Tybrandt, S. B. Kollipara, M. Berggren, Organic electrochemical transistors for signal amplification in fast scan cyclic voltammetry. *Sens. Actuators B* **195**, 651–656 (2014).
26. S. H. Kim, K. Hong, W. Xie, K. H. Lee, S. Zhang, T. P. Lodge, C. D. Frisbie, Electrolyte-gated transistors for organic and printed electronics. *Adv. Mater.* **25**, 1822–1846 (2012).
27. E. Said, N. D. Robinson, D. Nilsson, P.-O. Svensson, M. Berggren, Visualizing the electric field in electrolytes using electrochromism from a conjugated polymer. *Electrochem. Solid-State Lett.* **8**, H12–H16 (2005).
28. A. M. Nardes, M. Kemerink, R. A. J. Janssen, J. A. M. Bastiaansen, N. M. M. Kiggen, B. M. W. Langeveld, A. J. J. M. van Breemen, M. M. de Kok, Microscopic understanding of the anisotropic conductivity of PEDOT:PSS thin films. *Adv. Mater.* **19**, 1196–1200 (2007).
29. U. Lang, E. Müller, N. Naujoks, J. Dual, Microscopical investigations of PEDOT:PSS thin films. *Adv. Funct. Mater.* **19**, 1215–1220 (2009).
30. C. M. Palumbiny, C. Heller, C. J. Schaffer, V. Körstgens, G. Santoro, S. V. Roth, P. Müller-Buschbaum, Molecular reorientation and structural changes in cosolvent-treated highly conductive PEDOT:PSS electrodes for flexible indium tin oxide-free organic electronics. *J. Phys. Chem.* **118**, 13598–13606 (2014).
31. G. Buzsáki, in *Rhythms of the Brain* (Oxford Univ. Press, Oxford, 2006).
32. M. Gavaret, A. Trébuchon, F. Bartolomei, P. Marquis, A. McGonigal, F. Wendling, J. Regis, J.-M. Badier, P. Chauvel, Source localization of scalp-EEG interictal spikes in posterior cortex epilepsies investigated by HR-EEG and SEEG. *Epilepsia* **50**, 276–289 (2009).
33. J. W. Kowalski, M. Gawel, A. Pfeffer, M. Barcikowska, The diagnostic value of EEG in Alzheimer disease: Correlation with the severity of mental impairment. *J. Clin. Neurophysiol.* **18**, 570–575 (2001).
34. R. Hayashi, N. Hanyu, M. Shindo, F. Tamaru, N. Yanagisawa, Event-related potentials, reaction time, and cognitive state in patients with Parkinson's disease. *Adv. Neurol.* **60**, 429–433 (1993).
35. G. Pfurtscheller, A. Stancák, C. Neuper, Event-related synchronization (ERS) in the alpha band—An electrophysiological correlate of cortical idling: A review. *Int. J. Psychophysiol.* **24**, 39–46 (1996).
36. P. Gloor, G. Ball, N. Schaul, Brain lesions that produce delta waves in the EEG. *Neurology* **27**, 326–333 (1977).
37. R. Noriega, J. Rivnay, K. Vandewal, F. P. Koch, N. Stingelin, P. Smith, M. F. Toney, A. Salleo, A general relationship between disorder, aggregation and charge transport in conjugated polymers. *Nat. Mater.* **12**, 1038–1044 (2013).
38. S. Wang, M. Ha, M. Manno, C. Daniel Frisbie, C. Leighton, Hopping transport and the Hall effect near the insulator–metal transition in electrochemically gated poly(3-hexylthiophene) transistors. *Nat. Commun.* **3**, 1210 (2012).
39. Y. Tao, X. Xie, W. Lv, D. M. Tang, D. Kong, Z. Huang, H. Nishihara, T. Ishii, B. Li, D. Golberg, F. Kang, T. Kyotani, Q. H. Yang, Towards ultrahigh volumetric capacitance: Graphene derived highly dense but porous carbons for supercapacitors. *Sci. Rep.* **3**, 2975 (2013).
40. H. Toss, C. Suspène, B. Piro, A. Yassar, X. Crispin, L. Kergoat, M.-C. Pham, M. Berggren, On the mode of operation in electrolyte-gated thin film transistors based on different substituted polythiophenes. *Org. Electron.* **15**, 2420–2427 (2014).
41. E. Stavrinidou, P. Leleux, H. Rajaona, D. Khodagholy, J. Rivnay, M. Lindau, S. Sanaur, G. G. Malliaras, Direct measurement of ion mobility in a conducting polymer. *Adv. Mater.* **25**, 4488–4493 (2013).

Acknowledgments: We are grateful to J. Friedlein (University of Colorado) for fruitful discussions. **Funding:** This work was supported through grants by the Agence Nationale de la Recherche (MUSIC, PolyProbe), region Provence-Alpes-Côte d'Azur, the Fondation pour la Recherche Médicale, the Marie Curie ITN OLIMPIA, and Orthogonal Inc. J.R. and M.S. acknowledge a Marie Curie postdoctoral fellowship, and D.K. acknowledges a Simons Foundation postdoctoral fellowship. **Author contributions:** J.R. and G.G.M. conceived the research. M.F., M.S., D.A.K., D.K., M.R., X.S., and R.M.O. designed and/or fabricated devices. J.R., M.S., and P.L. measured and/or analyzed device characteristics and impedance. P.L. programmed acquisition software. P.L. and J.R. performed EEG recordings. J.R., D.K., A.W., M.F., and P.L. analyzed electrophysiology data. C. Bernard, C. Benar, and J.-M.B. designed the electrophysiology experiments and assisted with data interpretation. J.R. and G.G.M. wrote the manuscript, and all authors participated in manuscript input and editing. **Competing interests:** The authors declare that they have no competing interests.

Submitted 22 December 2014
Accepted 2 April 2015
Published 22 May 2015
10.1126/sciadv.1400251

Citation: J. Rivnay, P. Leleux, M. Ferro, M. Sessolo, A. Williamson, D. A. Koutsouras, D. Khodagholy, M. Ramuz, X. Strakosas, R. M. Owens, C. Benar, J.-M. Badier, C. Bernard, G. G. Malliaras, High-performance transistors for bioelectronics through tuning of channel thickness. *Sci. Adv.* **1**, e1400251 (2015).

Science Advances

High-performance transistors for bioelectronics through tuning of channel thickness

Jonathan Rivnay, Pierre Leleux, Marc Ferro, Michele Sessolo, Adam Williamson, Dimitrios A. Koutsouras, Dion Khodagholy, Marc Ramuz, Xenofon Strakosas, Roisin M. Owens, Christian Benar, Jean-Michel Badier, Christophe Bernard and George G. Malliaras

Sci Adv **1** (4), e1400251.
DOI: 10.1126/sciadv.1400251